Nonperturbative approach to the calculation of multiphonon Raman scattering in semiconductor quantum dots: Polaron effect

Rafael P. Miranda and Mikhail I. Vasilevskiy*
Centro de Física, Universidade do Minho, Campus de Gualtar, 4710-057 Braga, Portugal

Carlos Trallero-Giner
Departamento de Física Teórica, Universidad de La Habana, Vedado 10400, La Habana, Cuba
(Received 16 May 2006; published 21 September 2006)

Based on the polaron concept, a general nonperturbative approach to the calculation of the multiphonon Raman scattering cross section for semiconductor quantum dots (QDs) is proposed. Within this concept, the Raman scattering process consists of two virtual transitions in the exciton-polaron spectrum, one with absorption and the other with emission of a photon, which change the QD ground state (exciton vacuum with different number of phonons in the beginning and in the end of the process). By applying the formalism to a set of resonantly excited CdSe spherical QDs, it is found that the overall scattering spectra differ from the perturbation theory predictions, especially in what concerns the relative intensities of scattering processes of different order. The Raman spectra calculated in the framework of the polaron picture, without using any fitting parameters, show a better agreement with previously published experimental results, compared to those obtained within the perturbation theory approach. These results suggest that, even for materials with relatively small exciton-phonon coupling constants, the polaron effects can play an important role in the multiphonon Raman scattering of light by QDs.

DOI: 10.1103/PhysRevB.74.115317 PACS number(s): 78.67.Hc, 63.22.+m, 63.20.Kr

I. INTRODUCTION

In the past few years there has been an increased interest in studying the optical properties of quantum dot (QD) systems.[1] The interaction of electrons and holes with phonons is important for most of these properties since it determines hot carrier relaxation, influences light absorption and emission processes, and is responsible for the Raman scattering. The intensity of this interaction in QDs should be enhanced because of the electron and hole confinement. It leads to an increased probability of multiphonon processes. Moreover, owing to the discrete nature of the electron and hole energy spectra, the situation is described by polaronic quasiparticle excitations. The formation of electron-polaron states in QDs has been invoked in Refs. 2 and 3 in order to explain the spectral fine structure experimentally observed for self-assembled QDs using far-infrared spectroscopy of intraband electron transitions in magnetic field. (Note, however, that it required an unusually large value of the electron-phonon coupling constant to fit the spectra,[2] larger than one can expect for InAs.) Long decay times of electron states excited by absorption of far-infrared radiation in *n*-doped InAs/GaAs QDs, observed in Ref. 4, has been convincingly interpreted in terms of the electron-polaron formation.

As far as excitons are concerned, the importance of the polaron effect is less obvious because the exciton interaction with optical phonons through the Fröhlich-type coupling may be greatly reduced due to the partial compensation of the electron and hole charge densities in the dot. This affects, however, only the diagonal (or intralevel) exciton-phonon interaction, while the nondiagonal one (involving two different exciton states) is not subject to the compensation effect and can be quite important.[5] The absence of complete compensation in the diagonal coupling, too, is particularly drastic for the first order Raman cross section for spherical QDs. In the framework of the model considering simple electron and hole parabolic bands and particles confined inside infinite hard walls, the Raman scattering intensity due to LO-type phonons should be zero.[6] Only partial compensation between the electron and hole charge densities, implied by the observed nonzero scattering intensities, can be explained by the following reasons: (i) electron-hole Coulomb interaction, (ii) finite confinement barriers for the electron and hole, (iii) hole subband mixing, and (iv) formation of polaronic states. In all cases the Raman selection rule[6] is broken and different exciton channels with different spatial symmetry can participate in the Raman process.

Resonant Raman scattering (RRS) spectroscopy is probably the most direct method for probing the exciton-phonon interaction, particularly when absolute values of the intensity are measured.[7] It has been applied to QDs in several studies,[8–12] mostly with the objective to determine the characteristics of the confined and interface phonon modes participating in the first-order scattering. The authors of Refs. 8 and 9 measured also the higher order RRS spectra in nearly spherical CdSe and PbS nanocrystals. The multiphonon processes were considered theoretically in Refs. 13 and 14, and the obtained expressions for the RRS probability were applied to the modeling of the experimental data.[8,9]

The numerical results for CdSe nanocrystals, obtained on the basis of perturbation theory, reproduce the main trends in the experimental results, such as overtones characteristic of Raman selection rules, QD size effect, and the asymmetric line shapes of the Raman spectra.[13] Nevertheless, this theoretical model has only limited success when one attempts to describe the experimentally observed relative intensities of different phonon overtones, that is, to reproduce the overall measured spectrum at a given laser energy and for a specific

QD mean radius. In order to reach an agreement with the experimental data of Ref. 8, in Ref. 13 it was necessary to artificially multiply the intensities of the first order Raman by a factor of 13 and 2.55 for QDs with mean radius $\langle R\rangle = 1.9$ and 4.0 nm, respectively, while the third-order cross section of the QDs with $\langle R\rangle = 4.0$ nm was divided by a factor of 4.74. A reasonably good fit to the spectra[9] in Ref. 14 was achieved by assuming some nanocrystal interface imperfections, with several adjustable parameters involved. This study also treated the exciton-phonon interaction in the framework of perturbation theory. Even though the authors of the work[14] drew attention to the importance of nonadiabatic (i.e., nondiagonal) transitions and used a Green's function formalism, the final result for the scattering probability [Eq. (23) of Ref. 14] is just the same as one obtains using the standard perturbation theory (this expression is derived in the present paper).

A nonperturbative approach for the calculation of the one-phonon RRS probability for QDs, based on the polaron concept, was proposed in Ref. 15. Using the direct numerical procedure[5] for obtaining the polaron energy spectrum in a model QD, it was shown that, when either diagonal or nondiagonal coupling is sufficiently strong, the one-phonon Raman line shape and especially its resonant behavior differ considerably from the perturbation theory predictions.[15] However, the exciton-phonon coupling constants in Ref. 15 were treated as free parameters and significant differences between the exact and perturbation theory results appeared only for values that perhaps are too large for most QD materials. In the present work, the approach of Ref. 15 is generalized to multiphonon scattering processes and applied to RRS in spherical QDs made of a polar semiconductor material using calculated coupling constants. In this calculation, the electron-hole interaction, hole subband mixing, and hexagonal structure of the underlying material are included. Using these values and no fitting parameters, we show that the Raman spectrum of QDs with $\langle R\rangle = 1.9$ nm, calculated in the framework of the polaron concept, is in better agreement with the experimental results of Ref. 8 than that obtained within the perturbation theory approach.

The paper is organized as follows. In Sec. II, we derive expressions for the probability of Raman scattering of an arbitrary order using two approaches, (i) perturbation theory for both exciton-phonon and exciton-photon interactions, starting from bare exciton states, and (ii) exact consideration of the exciton-phonon interaction yielding polaron states and the second-order perturbation theory describing the coupling between the photon and the exciton-polaron states. In Sec. III, the application of both formalisms to the case of scattering in resonance with the lowest exciton states in QDs calculated using the spherical approximation for the Luttinger-Kohn Hamiltonian[16] is described. For this purpose, the exciton-phonon interaction matrix elements between the states of this octet are calculated taking into account the effects of light and heavy hole subband mixing, exchange interaction between the confined electron and hole, and possible hexagonal structure of the underlying QD material. The calculated results are presented and discussed in Sec. IV and Sec. V is devoted to concluding remarks.

II. GENERAL FORMALISM

A. Perturbation theory approach

Within this approach, it is assumed that purely excitonic states provide a good description of an optically excited QD (traditionally, the term "exciton" is used even when the Coulomb coupling energy of the electron-hole pair in the dot is small compared to the kinetic energy of each particle, which is the case in the strong confinement regime). Then, the k-phonon Raman scattering can be considered as a $(k+2)$th order process where an exciton created by absorption of an incident photon of frequency ω_I is successively scattered between available states through the generation (for the Stokes component) of k optical phonons, and finally exciton annihilation occurs by emitting a photon with frequency,

$$\omega_S = \omega_I - \sum_{\nu=1}^{N} r_\nu \omega_\nu, \tag{1}$$

where r_ν denotes the number of phonons of mode ν and frequency ω_ν created in the process. These numbers are such that

$$r_\nu \geqslant 0, \quad \nu = 1,2,\ldots,N, \quad \sum_{\nu=1}^{N} r_\nu = k. \tag{2}$$

The scattering matrix element can be easily written with the help of Feynman diagrams, like the one depicted in Fig. 1. In principle, it is necessary to consider all the possible diagrams obtained by permuting the order in which the interactions occur.[7,17] However, it is known that the diagrams in which the incident and scattered photons are not at the first and last vertices, respectively, can be safely neglected if the photon energy is large compared to that of phonons.[7] Thus for each possible combination of emitted phonons, the necessary matrix element can be written as

$$M_{\{r_\nu\}} = \frac{\prod_{\nu=1}^{N} r_\nu!}{k!} \sum_{\{\nu_k\}} \left\{ \sum_{\kappa_1,\kappa_2,\ldots,\kappa_{k+1}} \frac{\langle f|\hat{H}_{eR}^{(S)}|\kappa_{k+1}\rangle \left[\prod_{i=1}^{k} \langle \kappa_{i+1}|\hat{H}_{eL}^{(\nu_i)}|\kappa_i\rangle\right] \langle \kappa_1|\hat{H}_{eR}^{(I)}|i\rangle}{\prod_{i=0}^{k} (\hbar\omega_I - E_{\kappa_{i+1}})} \right\}, \tag{3}$$

where $\hat{H}_{eR}^{(I)}$ ($\hat{H}_{eR}^{(S)}$) denotes the Hamiltonian of interaction between an exciton and the incident (scattered) photon, $\hat{H}_{eL}^{(\nu_i)}$ is the Hamiltonian of interaction between an exciton and an optical phonon of mode ν_i, and the symbol $\Sigma_{\{\nu_k\}}$ represents a sum over all nonequivalent permutations of the indices $\nu_1, \nu_2, \ldots, \nu_k$, i.e., the sum extends over all topologically nonequivalent Feynman diagrams. The factor $\Pi_{\nu=1}^{N} r_\nu!/k!$ is the relative contribution of each nonequivalent diagram to the overall matrix element.

The initial and final states of the system are

$$|i\rangle = |0;m_1,m_2,\ldots,m_N;n_I,0_S\rangle \equiv |0;\{m_\nu\};n_I,0_S\rangle \tag{4}$$

and

$$|f\rangle = |0;m_1+r_1,m_2+r_2,\ldots,m_N+r_N;n_I-1,1_S\rangle \equiv |0;\{m_\nu\}';n_I-1,1_S\rangle, \tag{5}$$

where $|0\rangle$ represents the exciton vacuum, $\{m_\nu\}$ is a set of phonon occupation numbers determined by the temperature, and $n_{I,S}$ are the occupation numbers of the incident and scattered photons. The intermediate states, of energy

$$E_{\kappa_i} = E_{l_i} + \sum_{j=1}^{i-1} \hbar\omega_{\nu_j} \tag{6}$$

(where E_{l_i} is the energy of the exciton state $|l_i\rangle$), are described by the wave functions

$$|\kappa_i\rangle = |l_i;m_{\nu_1}+1,m_{\nu_2}+1,\ldots,m_{\nu_{i-1}}+1,m_{\nu_i},m_{\nu_{i+1}},\ldots,m_{\nu_k};n_I-1,0_S\rangle. \tag{7}$$

Let us assume that the QD material has a direct band structure and dipole transitions between the valence and conduction bands are allowed. Using the well-known expressions for the exciton-radiation and exciton-lattice interaction Hamiltonians[18] (see also Ref. 17), one obtains, in the dipole approximation,

$$\langle\kappa_1|\hat{H}_{eR}^{(I)}|i\rangle = \frac{e}{m_0 n}\left(\frac{2\pi\hbar n_I}{V\omega_I}\right)^{1/2} \mathbf{e}_I \cdot \mathbf{p}_{0l_1}, \tag{8}$$

$$\langle f|\hat{H}_{eR}^{(S)}|\kappa_{k+1}\rangle = \frac{e}{m_0 n}\left(\frac{2\pi\hbar}{V\omega_S}\right)^{1/2} \mathbf{e}_S \cdot \mathbf{p}_{0l_{k+1}}^{*}, \tag{9}$$

and

$$\langle\kappa_{i+1}|\hat{H}_{eL}^{(\nu_i)}|\kappa_i\rangle = (m_{\nu_i}+1)^{1/2}\hbar\omega_{\nu_i}\beta_{l_{i+1}l_i}^{(\nu_i)}. \tag{10}$$

In the above expressions, e and m_0 are the free-electron charge and mass, respectively, V denotes the scattering volume, n is the refractive index, $\mathbf{e}_{I,S}$ are the unit polarization vectors of the incident and scattered photons, $\mathbf{p}_{0l_i}$ is the momentum matrix element between the exciton states $|0\rangle$ and $|l_i\rangle$, and $\beta_{l_{i+1}l_i}^{(\nu_i)}$ denotes the exciton-phonon interaction constants for the phonon mode ν_i (normalized by the corresponding phonon energy). Within the envelope function approximation, the exciton wave functions can be expressed in the form

$$|l\rangle = \sum_{v,\sigma} C_{v,\sigma}^{(l)} \Psi_v^{(l)}(\mathbf{r}_h)\Psi_\sigma^{(l)}(\mathbf{r}_e)|v\rangle|\sigma\rangle, \tag{11}$$

where a simple conduction band of Γ_1 type has been assumed, σ denotes electron states in the conduction band with Bloch function $|\sigma\rangle$, v enumerates different valence bands (for example, four Γ_8 subbands) with the Bloch functions $|v\rangle$, $\Psi^{(l)}$ denotes the corresponding electron and hole envelope functions, and $C_{v,\sigma}^{(l)}$ are some coefficients. Then,

$$\mathbf{p}_{l0} = \mathbf{p}_{0l}^{*} = \sum_{v,\sigma} C_{v,\sigma}^{(l)} \langle v|\hat{\mathbf{p}}|\sigma\rangle \int \Psi_v^{(l)}(\mathbf{r})\Psi_\sigma^{(l)}(\mathbf{r})d\mathbf{r}, \tag{12}$$

with $\langle v|\hat{\mathbf{p}}|\sigma\rangle$ representing the momentum matrix element between the electron states of the bottom of the conduction band and the top of the valence band. The explicit form of $\beta_{l_{i+1}l_i}^{(\nu_i)}$ depends on the interaction mechanism, which will be specified below.

The scattering probability can be calculated using Fermi's "golden rule" and summing over all possible sets $\{r_\nu\}$. When $\mathbf{e}_I \| \mathbf{e}_S$, the transition dipole moment preserves its orientation between two interactions with photons and, hence, the scalar products in Eqs. (8) and (9) can be replaced by z projection of the momentum, p_{0l}. In this case, the scattering probability for the kth order process can be written as

$$p_k = \frac{2\pi}{\hbar}\left(\frac{e}{m_0 n}\right)^4\left(\frac{2\pi\hbar}{V}\right)^2 \frac{n_I}{\omega_I\omega_S}\frac{1}{(k!)^2} \times \sum_{\{r_\nu\}} \left\{ \prod_{\nu=1}^{N}\left[(r_\nu!)^2(\hbar\omega_\nu)^{2r_\nu}\prod_{i=1}^{r_\nu}(m_\nu+i)\right] \times \left| \sum_{\{\nu_k\}} \left[\sum_{l_1,l_2,\ldots,l_{k+1}} \frac{p_{0l_1}p_{0l_{k+1}}^{*}\prod_{i=1}^{k}\beta_{l_{i+1}l_i}^{(\nu_i)}}{\prod_{i=0}^{k}\left(\hbar\omega_I - \sum_{j=1}^{i}\hbar\omega_{\nu_j} - E_{l_{i+1}}\right)} \right] \right|^2 \times \delta(\hbar\omega_I - \hbar\omega_S - E_{\{r_\nu\}}) \right\}, \tag{13}$$

where

$$E_{\{r_\nu\}} = \sum_{\nu=1}^{N} r_\nu\hbar\omega_\nu \tag{14}$$

and the term $\Pi_{\nu=1}^{N}[(\hbar\omega_\nu)^{2r_\nu}\Pi_{i=1}^{r_\nu}(m_\nu+i)]$ arises from the possibility of having several emitted phonons of the same mode.

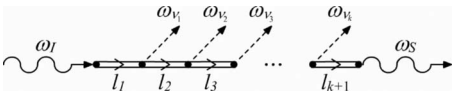

FIG. 1. Typical diagram representing a kth order Raman scattering process.

As it has been mentioned, in the initial state the phonon occupation numbers correspond to thermal equilibrium. Therefore it is necessary to perform a thermodynamical average so that the outcome of Eq. (13) is physically meaningful. Taking into account the following expression:

$$\left\langle \prod_{i=1}^{r_\nu} (m_\nu + i) \right\rangle = \frac{r_\nu!}{\left[1 - \exp\left(-\frac{\hbar\omega_\nu}{k_B T}\right)\right]^{r_\nu}}, \tag{15}$$

it can be obtained

$$p_k = \frac{2\pi}{\hbar}\left(\frac{e}{m_0 n}\right)^4 \left(\frac{2\pi\hbar}{V}\right)^2 \frac{n_I}{\omega_I \omega_S} S_k, \tag{16}$$

where

$$S_k = \frac{1}{(k!)^2} \sum_{\{r_\nu\}} \left\{ \prod_{\nu=1}^{N} \frac{(r_\nu!)^3 (\hbar\omega_\nu)^{2r_\nu}}{\left[1 - \exp\left(-\frac{\hbar\omega_\nu}{k_B T}\right)\right]^{r_\nu}} \right.$$
$$\times \left| \sum_{\{\nu_k\}} \left[\sum_{l_1, l_2, \ldots, l_{k+1}} \frac{p_{0l_1} p^*_{0l_{k+1}} \prod_{i=1}^{k} \beta^{(\nu_i)}_{l_{i+1} l_i}}{\prod_{i=0}^{k} \left(\hbar\omega_I - \sum_{j=1}^{i} \hbar\omega_{\nu_j} - E_{l_{i+1}}\right)} \right] \right|^2$$
$$\left. \times \delta(\hbar\omega_I - \hbar\omega_S - E_{\{r_\nu\}}) \right\}. \tag{17}$$

Let us notice that this expression (for $T=0$) was formerly derived in Ref. 13. It also corresponds to that used in Ref. 14 where it is called *leading term approximation*.

In a Raman scattering experiment, the measured quantity is not the scattering probability, but the differential cross section. For a Stokes process, this quantity is given by[17]

$$\frac{d^2\sigma}{d\Omega d\omega_S} = p\left(\frac{n}{c}\right)^4 V^2 \frac{\omega_S^2}{8\pi^3} \frac{1}{n_I}, \tag{18}$$

where c is the velocity of light in vacuum. Inserting Eq. (16) into Eq. (18) yields

$$\frac{d^2\sigma^{(k)}}{d\Omega d\omega_S} = \hbar\left(\frac{e}{m_0 c}\right)^4 \frac{\omega_S}{\omega_I} S_k. \tag{19}$$

B. Raman scattering in the polaron picture

Strictly speaking, the formalism described in the previous section is only valid when the exciton-phonon interaction constants are small. When this is not the case, it is necessary to tackle the problem in a nonperturbative way, considering the eigenstates of the coupled exciton-phonon many-body system. These eigenstates are the stationary states of the exciton-polaron. In this framework, the multiphonon Raman scattering is always a second-order process where a superposition of different polaron states is created by absorption of a photon of frequency ω_I and then the polaron annihilates by emitting a photon of a different frequency, ω_S, given by Eq. (1). Such a process leaves behind the system with no excitons and a certain (different) number of free phonons. The overall scattering probability is now given by

$$p = \frac{2\pi}{\hbar} \frac{1}{Z} \sum_{i,f} \left\{ \exp\left(-\frac{E_i}{k_B T}\right) \left| \sum_{\kappa} \frac{\langle f|\hat{H}^{(S)}_{eR}|\kappa\rangle\langle\kappa|\hat{H}^{(I)}_{eR}|i\rangle}{E_\kappa - E_i - \hbar\omega_I} \right|^2 \right.$$
$$\left. \times \delta(E_f - E_i - \hbar\omega_I) \right\}, \tag{20}$$

where an average over the initial states (free phonons with occupation numbers $\{m_\nu\}$) and a sum over the final ones have already been included. These states are the same as in the perturbation theory approach, so the energy E_i must be interpreted as free phonon's energy only, i.e.,

$$E_i \equiv E_{\{m_\nu\}} = \sum_{\nu=1}^{N} \left(m_\nu + \frac{1}{2}\right)\hbar\omega_\nu. \tag{21}$$

Accordingly, the partition function of the initial states, Z, is given by

$$Z = \sum_{\{m_\nu\}} \exp\left(-\frac{E_{\{m_\nu\}}}{k_B T}\right). \tag{22}$$

The intermediate states, however, are different in this polaron picture,

$$|\kappa\rangle = |\alpha; n_I - 1, 0_S\rangle. \tag{23}$$

In this equation, $|\alpha\rangle$ denotes the αth exciton-polaron state of energy E_α. It is convenient to express these states as linear combinations of the eigenstates of the uncoupled exciton and phonons, $|l;\{m_\nu\}\rangle$:

$$|\alpha\rangle = \sum_{l,\{m_\nu\}} c^{(\alpha)}_{l,\{m_\nu\}} |l;\{m_\nu\}\rangle. \tag{24}$$

In some cases the coefficients of this expansion and the polaron energy levels can be found analytically, for example, within the independent boson model.[19] This is not possible, however, if both diagonal and nondiagonal exciton-phonon interactions are included. Then, in principle, the problem can be solved numerically as proposed in Ref. 5. If the system's Hamiltonian is truncated by including a certain (relatively small) number of phonons allowed for each mode, then it can be easily diagonalized, yielding a very accurate solution for the polaron energies (in a certain spectral range) and the expansion coefficients $c^{(\alpha)}_{l,\{m_\nu\}}$.[5]

Using Eqs. (23) and (24), the expressions for the necessary matrix elements can be obtained in the same way as for Eqs. (8) and (9), yielding

$$\langle\kappa|\hat{H}^{(I)}_{eR}|i\rangle = \frac{e}{m_0 n}\left(\frac{2\pi\hbar n_I}{V\omega_I}\right)^{1/2} \sum_{l} (c^{(\alpha)}_{l,\{m_\nu\}})^* \mathbf{e}_I \cdot \mathbf{p}_{0l} \tag{25}$$

and

$$\langle f|\hat{H}_{eR}^{(S)}|\kappa\rangle = \frac{e}{m_0 n}\left(\frac{2\pi\hbar}{V\omega_S}\right)^{1/2}\sum_l c_{l,\{m_\nu\}'}^{(\alpha)}\mathbf{e}_S\cdot\mathbf{p}_{0l}^*. \quad (26)$$

For the case of parallel polarizations, the scattering probability can therefore be written as

$$p = \frac{2\pi}{\hbar}\left(\frac{e}{m_0 n}\right)^4\left(\frac{2\pi\hbar}{V}\right)^2\frac{n_I}{\omega_I\omega_S}\tilde{S}, \quad (27)$$

where

$$\tilde{S} = \frac{1}{Z}\sum_{\{m_\nu\}}\exp\left(-\frac{E_{\{m_\nu\}}}{k_B T}\right) \times\sum_{\{r_\nu\}}\left\{\left|\sum_\alpha\frac{\sum_{l,l'}p_{0l}p_{0l'}^*(c_{l,\{m_\nu\}}^{(\alpha)})^* c_{l',\{m_\nu\}'}^{(\alpha)}}{E_\alpha - E_{\{m_\nu\}} - \hbar\omega_I}\right|^2 \times\delta(\hbar\omega_I - \hbar\omega_S - E_{\{r_\nu\}})\right\}. \quad (28)$$

Thus the differential cross section in this approach takes the form

$$\frac{d^2\sigma}{d\Omega d\omega_S} = \hbar\left(\frac{e}{m_0 c}\right)^4\frac{\omega_S}{\omega_I}\tilde{S}. \quad (29)$$

Once the polaron eigenstates are known, this formula is very convenient for numerical calculations.

III. APPLICATION TO SPHERICAL QDS

Within the effective mass approximation based on the Luttinger-Kohn Hamiltonian, the lowest exciton states in spherical QDs made of materials such as CdSe belong to the $1s_e 1S_{3/2}$ octet.[20] These states are all degenerate in the simplest approximation (considering a perfectly spherical QD, infinite barriers, cubic structure of the underlying material, and no electron-hole interaction) and are designated by the electron spin projection, $s_z = \pm 1/2$, and the hole momentum projection, $M = \pm 1/2, \pm 3/2$. Their energy is given by[20,21]

$$E(R) = E_g + \frac{\pi^2\hbar^2}{2m_e^2 R^2} + \frac{\kappa^2\hbar^2}{2m_{hh}^2 R^2}, \quad (30)$$

where E_g is the bulk band gap energy, R the QD radius, m_e and m_{hh} are the electron and heavy hole effective masses, respectively, and κ is the first root of the equation

$$j_0(\kappa)j_2(\beta^{1/2}\kappa) + j_2(\kappa)j_0(\beta^{1/2}\kappa) = 0, \quad (31)$$

with j_l the spherical Bessel functions of order l and $\beta = m_{lh}/m_{hh}$ the ratio of the light and heavy hole effective masses. Explicit expressions for the electron and hole wave functions are given in the Appendix. In the strong confinement regime, the Coulomb interaction between the electron and hole can be considered as a perturbation and, to the lowest order, it leads to an equal shift of all eight exciton states $|s_z, M\rangle$ by a value $U_C = -\chi e^2/(\epsilon_0 R)$, where ϵ_0 is the static dielectric constant of the QD material and the coefficient χ varies between 1.77 and 1.90 depending on the value of β. In this approximation, the exciton wave functions remain in the form of products of the corresponding electron and hole ones. The eightfold degenerate state is split into five energy levels when the electron-hole exchange interaction and the intrinsic crystal field (present for QD materials with hexagonal structure) are taken into account. These effects were considered in detail in Ref. 21. Using the notation proposed in this work, the exciton states with different total angular momentum, $0^{U,L}$, $\pm 1^{U,L}$, and ± 2, have the following energies [with respect to the value given by Eq. (30) with U_C added],

$$E_{0^{U,L}} = \frac{1}{2}\eta + \frac{\Delta}{2} \pm 2\eta,$$

$$E_{\pm 1^{U,L}} = \frac{1}{2}\eta \pm \sqrt{4\eta^2 + \frac{\Delta^2}{4} - \eta\Delta},$$

$$E_{\pm 2} = -\frac{3}{2}\eta - \frac{\Delta}{2}. \quad (32)$$

In Eq. (32), "+" corresponds to the upper (U) state and "−" to the lower one (L),

$$\Delta = \Delta_{cr}\int_0^R\left[R_0^2(r) - \frac{3}{5}R_2^2(r)\right]r^2 dr, \quad (33)$$

Δ_{cr} is the value of the crystal field splitting, and

$$\eta = \frac{\varepsilon_{exc}a_0^3}{3\pi R}\int_0^R\sin^2(\pi r/R)\left[R_0^2(r) + \frac{1}{5}R_2^2(r)\right]dr, \quad (34)$$

with ε_{exc} the exchange strength constant and a_0 the lattice constant. The radial functions $R_0(r)$ and $R_2(r)$ are given in the Appendix. Note that the states with "±" remain twofold degenerate. Figure 2 shows the radial dependence of the spectral density of states of the exciton-polaron spectra of CdSe QDs, calculated at room temperature. For comparison, the lower and upper bounds of the energies (32) are also shown. The parameters used in the calculation are given in Table I. They were taken from Refs. 21–24, except for the value of β which was chosen rather arbitrarily in the middle of the broad range of data that appear in the literature for this parameter. As it can be seen from the inset in Fig. 2, five levels that belong to the $1s_e 1S_{3/2}$ octet occupy an energy region not exceeding 20 meV in width. Notice that for larger radii ($4\ \text{nm} \lesssim R \lesssim 5\ \text{nm}$, not considered here), the splitting produced by the exchange interaction is small and the crystal field leads to two levels separated by a few meV [the limit $\eta \to 0$ in Eqs. (32)].

The spatial confinement effect on optical phonons in spherical QDs has been considered theoretically in several works,[25–27] in the framework of a continuum model originally proposed in Ref. 28 and successfully used for a wide range of semiconductor nanostructures. The confinement leads to the quantization of optical phonon modes that, in general, have a mixed longitudinal-transverse-interface nature and are classified according to three spherical quantum numbers n_p, l_p, and m_p. If the QD material is a polar semi-

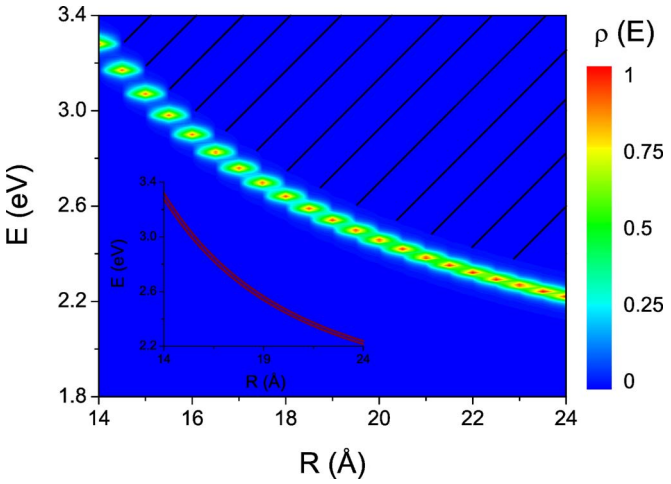

FIG. 2. (Color online) Radial dependence of the spectral density of exciton-polaron states, $\rho=\frac{1}{\pi}\,\mathrm{Im}\,G$ (G is the Green's function defined in Ref. 5), calculated for CdSe QDs ($T=300$ K). Each spot corresponds to a certain QD radius which varies discretely ($\Delta R=0.5$ Å) and represents the variation of ρ only along the energy axis. The shaded area of the E-R plane represents the region where numerical calculations of the polaron spectrum have not been performed. For comparison, the lower and upper bounds of the bare exciton energies (32) are shown in the inset.

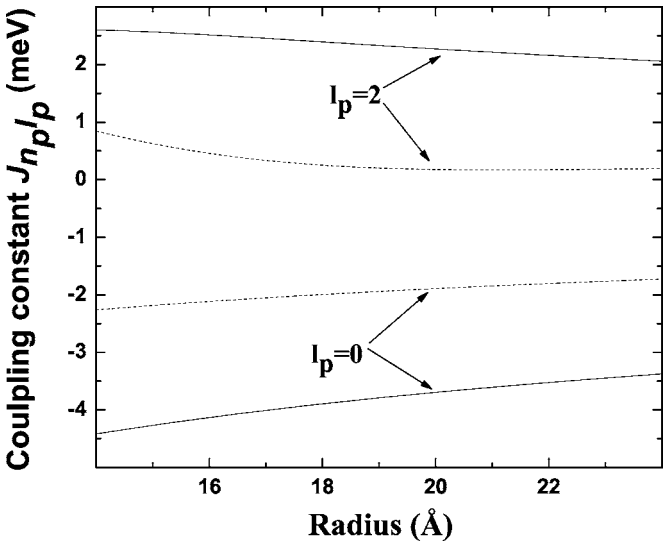

FIG. 3. Coupling constants $J_{n_p l_p}$ as functions of the dot radius, calculated for CdSe spherical QDs embedded in a matrix with $\epsilon_h=2.25$. The solid line represents the phonon modes with $n_p=1$ and dashed line the $n_p=2$ modes.

conductor, the exciton-phonon interaction occurs mostly through the Fröhlich-type mechanism, with the matrix elements given by

$$B_{ll'}^{(n_p l_p m_p)} = \langle l' | e[\varphi_{n_p l_p m_p}(\mathbf{r}_h) - \varphi_{n_p l_p m_p}(\mathbf{r}_e)] | l \rangle, \qquad (35)$$

where $\varphi_{n_p l_p m_p}(\mathbf{r})$ is the electrostatic potential associated with the phonon mode $(n_p l_p m_p)$. Because of the symmetry of the electron and hole envelope functions of the $1s_e 1S_{3/2}$ states, only phonons with $l_p=0,2$ give nonzero matrix elements (35). In the basis of the $0^{U,L}$, $\pm 1^{U,L}$, and ± 2 states, the exciton-phonon interaction matrix for $l_p=0$ is diagonal, with the coupling constant given by

$$J_{n_p 0} = \frac{C_F}{\sqrt{4\pi}} \int_0^R [R_0^2(r) + R_2^2(r) - \psi_e^2(r)] \Phi_{n_p 0}(r) r^2 dr, \quad (36)$$

where $\Phi_{n_p 0}(r)$ is the (dimensionless) radial part of the function $\varphi_{n_p l_p m_p}(\mathbf{r})$ with $l_p=m_p=0$ and different n_p (see Appendix), $\psi_e(r)$ denotes the radial part of the electron wave function given in the Appendix, and $C_F=e\sqrt{2\pi\hbar\omega_{LO}(\epsilon_\infty^{-1}-\epsilon_0^{-1})/R}$ is the Fröhlich constant ($\hbar\omega_{LO}$ and ϵ_∞ are the bulk longitudinal optical phonon frequency and high frequency dielectric constant of the QD material). The exciton-phonon interaction matrices for $l_p=2$ are given in the Appendix. All the nonzero matrix elements are expressed in terms of a single constant (for each n_p),

$$J_{n_p 2} = \frac{C_F}{\sqrt{5\pi}} \int_0^R R_0(r) R_2(r) \Phi_{n_p 2}(r) r^2 dr. \qquad (37)$$

Figure 3 shows the radial dependence of the coupling constants $J_{n_p 0}$ and $J_{n_p 2}$ for $n_p=1,2$, calculated for CdSe QDs embedded in a matrix with a high frequency dielectric constant $\epsilon_h=2.25$. The parameters of optical phonons for bulk CdSe used in these calculations are the same as Ref. 27.

It is clear from Fig. 3 that the constants $J_{n_p 0}$ and $J_{n_p 2}$ are larger (in absolute value) for $n_p=1$. In fact, generally they decrease monotonically when n_p increases, at least for the values of β close to that used in this work. Since the exciton-phonon interaction parameters are completely determined by these quantities (within the present model considering only the lowest exciton octet state), it is not difficult to foresee that the most important phonon modes for the Raman scattering are those with $n_p=1$ and $l_p=0,2$. Because of the computational limitations, we did not perform calculations with all six $n_p=1$, $l_p=0,2$ modes included explicitly. In order to reduce the size of the Hamiltonian matrix, we considered just three phonon modes, those with $l_p=0$, $l_p=2$, and $m_p=0$, and a third "unified" one which represents the remaining modes with $l_p=2$ and $m_p\neq 0$. For the latter, in order to preserve the Hermiticity of the Hamiltonian, we considered that

$$B^{(12,m_p\neq 0)} = B^{(12,1)} - B^{(12,-1)} + B^{(12,2)} + B^{(12,-2)}, \qquad (38)$$

i.e.,

TABLE I. CdSe parameters used in the calculations.

Parameter	Value
E_g (eV)	1.74,[a] 1.82[b]
m_e	$0.12m_0$
m_{lh}	$0.30m_0$
β	0.17
ϵ_0	9.7
ϵ_∞	6.2
$\varepsilon_{exc}a_0^3$ (meV nm^3)	36
Δ_{cr} (meV)	25

[a]At 300 K.
[b]At 77 K.

$$B^{(12,m_p\neq 0)} = J_{12}\begin{pmatrix} 0 & 0 & a^+ & -a^- & -a^+ & -a^- & -1 & i \\ 0 & 0 & -a^+ & a^- & -a^+ & -a^- & -1 & -i \\ a^+ & -a^+ & 0 & 0 & -\sqrt{2}c & \sqrt{2}b & \sqrt{2}a^- & 0 \\ -a^- & a^- & 0 & 0 & -\sqrt{2}b & -\sqrt{2}c & \sqrt{2}a^+ & 0 \\ -a^+ & -a^+ & -\sqrt{2}c & -\sqrt{2}b & 0 & 0 & 0 & \sqrt{2}ia^- \\ -a^- & -a^- & \sqrt{2}b & -\sqrt{2}c & 0 & 0 & 0 & -\sqrt{2}ia^+ \\ -1 & -1 & \sqrt{2}a^- & \sqrt{2}a^+ & 0 & 0 & 0 & 0 \\ -i & i & 0 & 0 & -\sqrt{2}ia^- & \sqrt{2}ia^+ & 0 & 0 \end{pmatrix}, \tag{39}$$

where the constants $a^{\pm}$, b, and c are defined in the Appendix.

The exciton-phonon coupling matrices presented above were used to calculate the polaron states generated by the $1s_e1S_{3/2}$ octet of bare exciton levels. As it can be seen from Fig. 2, these states populate rather densely the energy region above a certain minimum value characteristic of each QD radius. Obviously, only some of these states have been calculated correctly because of the truncation procedure used to diagonalize the (infinite) Hamiltonian matrix. Their energies are shown in Fig. 2 while the rest of the *E-R* plane is shaded since no results are available for this region from the present calculation.

IV. RESULTS AND DISCUSSION

As it was mentioned in the previous section, for large QD radii the splitting of the $1s_e1S_{3/2}$ state owing to the exchange interaction is small and the crystal field produces two levels separated only by a few meV. On the other hand, the next groups of exciton states, such as $1s_e1P_{3/2}$ (optically inactive) and $1s_e2S_{3/2}$ (optically active), are rather close to the $1s_e1S_{3/2}$ one.[20] Neglecting any splitting within these groups, we first consider a simplified model for CdSe QDs, with only two optically active exciton levels of energies $E_1=2.6$ eV and $E_2=2.7$ eV, coupled to a single $l_p=0$ phonon mode of energy $\hbar\omega_1=25.8$ meV. For this model, the exciton-phonon coupling constants β_{11}, β_{22}, and β_{12} were varied and calculations were performed with the aim to study the effect of the different parameters. The relative intensity of the second- and first-order scattering processes was computed as a function of the incident energy and either nondiagonal or diagonal exciton-phonon interaction constants. First, the coupling constants were chosen in the region of small values, where two approaches described in Sec. II should give the same results. While varying the nondiagonal coupling constant, the diagonal ones were kept at fixed values given in Ref. 29 for a spherical QD with $R=2$ nm (and vice versa). The results for room temperature are presented in Figs. 4 and 5. It is clear that, when all the interaction constants are small, two approaches are equivalent (Fig. 4). However, if at least one of them increases the results come to differ substantially. This is most clearly seen for the diagonal coupling (Fig. 5).

The first and second order Raman peaks of Fig. 4 show the outgoing resonances at 2.625 and 2.725 eV, while Fig. 5

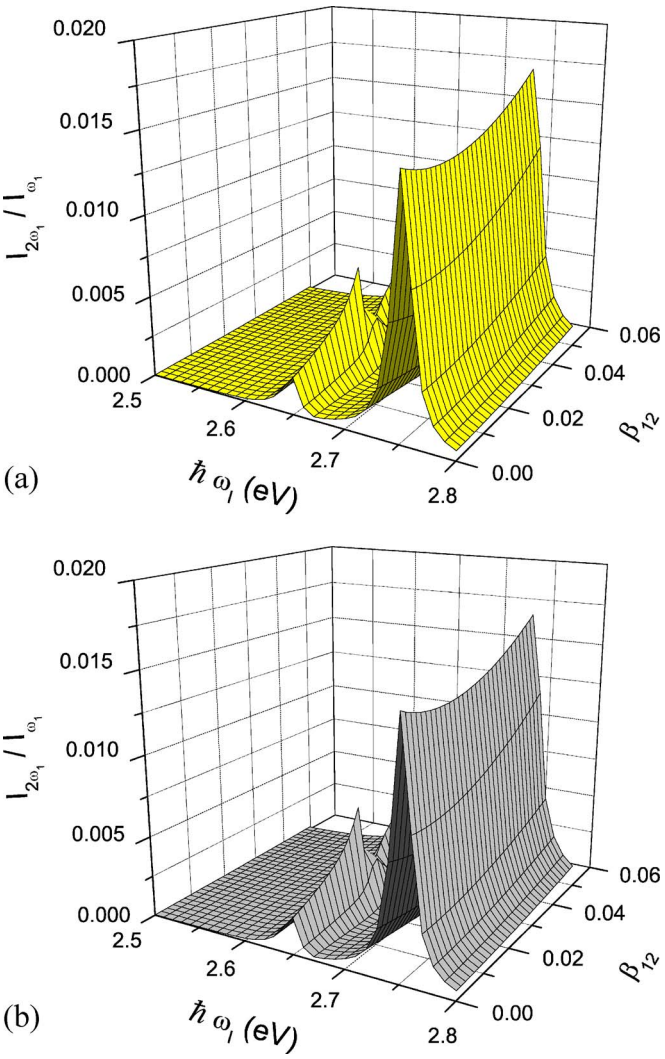

FIG. 4. (Color online) Relative intensity of the second- and first-order scattering processes as a function of the incident energy and the nondiagonal exciton-phonon interaction constant for a QD with two optically active exciton levels ($E_1=2.6$ eV, $E_2=2.7$ eV, and dipole transition matrix elements $p_{01}=p_{02}$) coupled to a single optical phonon mode ($\hbar\omega_1=25.8$ meV), calculated in the perturbation theory (a) and polaron (b) approaches. The diagonal coupling constants were kept at fixed values of $\beta_{11}=0.02$ and $\beta_{22}=0.04$ (Ref. 29).

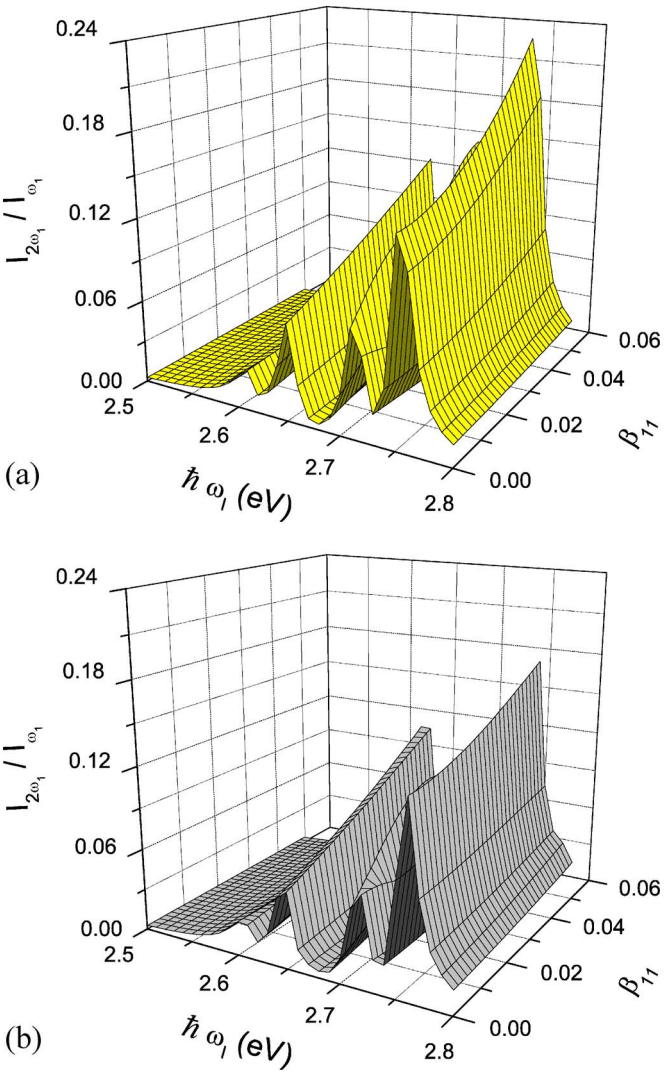

FIG. 5. (Color online) Relative intensity of the second and first-order scattering processes as a function of the incident energy and the diagonal exciton-phonon interaction constants for the QD of Fig. 4, calculated in the perturbation theory (a) and polaron (b) approaches. The nondiagonal coupling constant was kept at a fixed value of $\beta_{12}=0.3$ (Ref. 29) and it was assumed that $\beta_{22}=2\beta_{11}$.

presents [as well as the spectra shown in Figs. 6(a) and 6(b) do] both the incoming and outgoing resonances. The relative intensity of the second order peak grows with the increase of β_{11} and β_{12}, which can be interpreted as the result of a stronger confinement (smaller R, Fig. 3). The perturbation theory approach overestimates this enhancement [compare Figs. 5(a) and 5(b)]. Notice also that this result is based on the consideration of just two bare exciton states involved in the scattering (we shall return to this point in the end of this section).

Including a second bare phonon mode, of energy $\hbar\omega_2=25$ meV, within the same simplified two-state model produces more realistic Raman line shapes [it is known that the asymmetric line shapes of Raman spectra of QDs are due to the contribution of confined phonon modes with larger n_p (Ref. 10 and 30)]. Figure 6 shows the results calculated for two different values of the exciton energy level separation, ΔE. Qualitatively, the spectra calculated in the two approaches do not differ much, even when the interlevel spacing is of the order of the phonon energies. Notice, however, that in this case the first-order peak obtained in the polaron approach is slightly broader than that calculated using the perturbation theory approach. This effect is related to the somewhat different contribution of the second bare phonon mode, which is predicted by the two calculation schemes.

As the level separation ΔE approaches the phonon frequency ($\Delta E \approx \hbar\omega_{1,2}$), the condition of double (incoming and outgoing) resonance is reached and an enhancement of the first order Raman signal is obtained.[31] This effect is clearly seen if Figs. 6(a) and 6(b) are compared to Figs. 6(c) and 6(d) where an increase of the Raman signal by more than one order of the magnitude is obtained. It is independent of the formalism used because, as emphasized in Ref. 5, no qualitative changes occur in the polaron spectrum when the phonon energy matches the difference between the bare exciton state energies.

In order to obtain theoretical Raman scattering spectra, suitable for a direct comparison with the experimental data obtained for smaller CdSe QDs excited in resonance with the $1s_e1S_{3/2}$ exciton state,[8] it is necessary to consider the exciton octet coupled to the most important phonon modes and to include the effects of hole band mixing, exchange interaction, hexagonal structure, and phonon confinement, as explained in Sec. IV. Additionally, the size distribution of the QDs, always present in real samples, must be taken into account. The Raman spectra calculated assuming a Gaussian distribution of radii, with a mean value of 1.9 nm and a standard deviation of 10%, are shown in Fig. 7 along with the experimental data from Ref. 8. The calculated Raman spectra reproduce the main trends of the experimental result. One can see that the spectra are better described within the polaronic picture here developed than using the standard perturbation theory. In particular, the relative intensity of two spectral peaks, obtained within the polaron concept, is clearly in a better agreement with the experimental data than that calculated along the lines of the perturbation theory. In our opinion, the reasons for the remaining discrepancy are (i) the limited number of phonon modes included in the calculation, (ii) the neglecting of higher energy exciton states, and (iii) the uncertainty in the experimental data related to the necessity to subtract the luminescence related background and the optical absorption corrections in the measured Raman spectra. Including phonon modes with the same symmetry and higher n_p, which have slightly lower frequencies and are more weakly coupled to excitons, would certainly result in a better reproduction of the Raman peak's shape.[10,30] Taking into consideration higher energy bare exciton states, such as the $(1s_e1P_{3/2})$ octet, would allow the participation of phonons with $l_p=1,3$ in the higher order scattering (but not in the first order process), therefore increasing its relative intensity. Both approaches presented in this paper, the exact polaronic one and the perturbation theory approximation, should reproduce this effect. However, it seems technically impossible, for the computational reason, to include much more phonon and/or exciton modes in the exact diagonalization scheme used to calculate the polaron states. Within the scope of this work, we have demonstrated the importance of

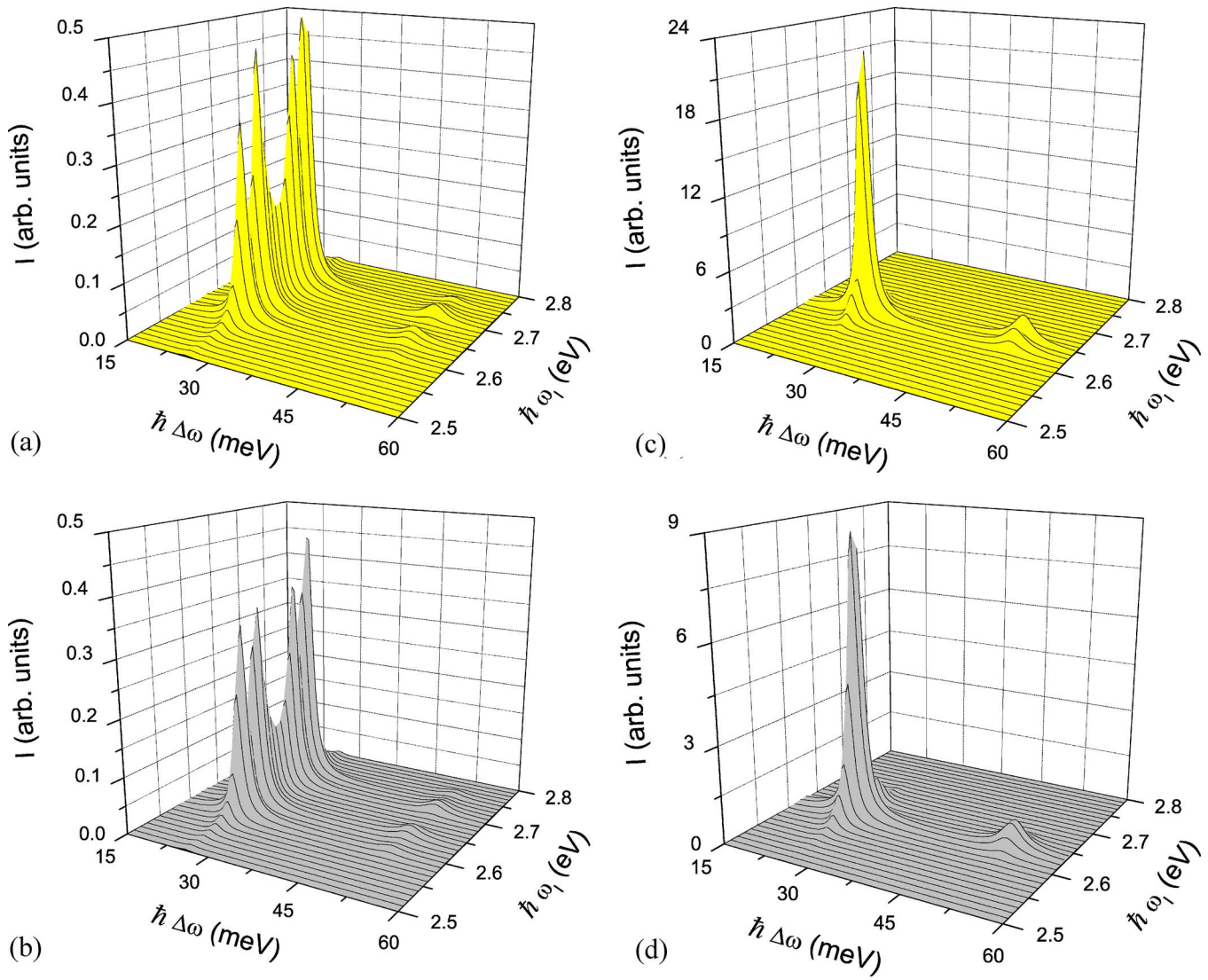

FIG. 6. (Color online) Raman scattering spectra (up to the second order) for a QD with two optically active exciton levels (E_1 =2.6 eV, $E_2=E_1+\Delta E$, and dipole transition matrix elements $p_{01}=p_{02}$) coupled to two optical phonon modes ($\hbar\omega_1=25.8$ meV and $\hbar\omega_2$ =25 meV), calculated in the perturbation theory [(a) and (c)] and polaron [(b) and (d)] approaches. The exciton-phonon interaction constants used are from Ref. 29: $\beta_{11}^{(1)}=0.02$, $\beta_{22}^{(1)}=0.04$, $\beta_{12}^{(1)}=0.3$, $\beta_{11}^{(2)}=0.01$, $\beta_{22}^{(2)}=0.07$, and $\beta_{12}^{(2)}=0.02$. Graphs (a) and (b) correspond to ΔE =100 meV, while for graphs (c) and (d) $\Delta E=25$ meV.

the polaron effect in the Raman scattering by realistic quantum dots.

Another important point deserves to be discussed in this respect. Several papers, as well as our calculated results presented in Fig. 3, affirm that the exciton-phonon interaction increases with the decrease of the QD size. However, this is not at all obvious if one compares experimental multiphonon Raman spectra of QDs of different radii. For instance, the spectra measured in Ref. 8 for QDs of mean radius $\langle R\rangle$ =4.0 nm show three phonon lines, while the third peak is not seen in the data for $\langle R\rangle=1.9$ nm (in both cases the spectra were recorded in resonance with the first absorption peak). Does it imply that the exciton-phonon coupling constants increase with the QD size, perhaps because of an additional decompensation of the electron and hole clouds owing to the stronger exciton effect (and weaker confinement) in the larger dots? Calculations performed within the weak confinement model,[32] and the necessity to recover the macroscopic limit when $R\rightarrow\infty$, teach us that the answer to the above question is no. The higher number of multiphonon Raman peaks appearing in the spectra of larger QDs (and even a higher number for bulk semiconductors) is explained for the larger number of intermediate exciton states involved in the scattering. The importance of including all possible states of the electron-hole pairs, in order to correctly describe the higher order multiphonon Raman peaks, was predicted in the past for systems other than QDs.[33]

V. CONCLUSIONS

We have proposed a general nonperturbative approach to the calculation of the multiphonon Raman scattering cross section for semiconductor QDs, taking into account the polaron effect. The results obtained using the simplified two-

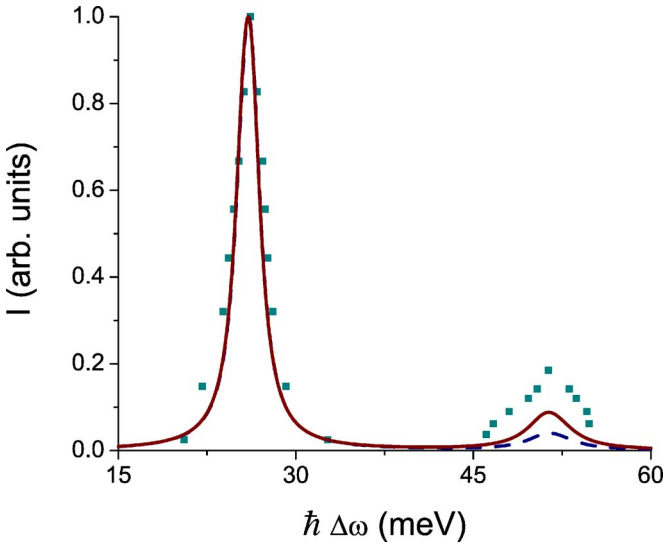

FIG. 7. (Color online) Raman scattering spectra (up to the second order) calculated at $T=77$ K in the perturbation theory (dashed line) and polaron (solid line) approaches for CdSe QDs with a mean radius of 1.9 nm and a size dispersion of 10%. The excitation energy is $\hbar\omega_l=2.572$ eV; additional parameters are given in Table I. The squares are experimental data from Ref. 8. Each curve is normalized to the height of the main (1LO) peak whose absolute value is approximately 30% lower in the polaron approach.

level model with adjustable exciton-phonon coupling constants reveal several important features which cannot be properly understood within the standard perturbation theory approach. In particular, if either diagonal or nondiagonal coupling constants exceed certain values (typically 0.1 for β_{12} and 0.05 for β_{11}), the relative intensity between the second- and first-order scattering processes deviates considerably from the perturbation theory predictions. Moreover, this also applies, under certain excitation conditions, to the relative contributions of the various phonon modes which participate in the scattering. The comparison between the Raman spectra calculated using the two approaches (with no fitting parameters involved) and experimental data obtained for small spherical CdSe QDs[8] strongly supports the importance of the polaron effect on the multiphonon Raman scattering, even for moderated values of the exciton-phonon coupling rates. The relative intensities of Raman peaks of different order, as well as those of the different incoming or outgoing resonances in the excitation spectra, can be used for evaluation of the exciton-phonon interaction constants in QDs, and this has to be done within the polaron concept. At the same time, it is important to include more intermediate polaron states when considering higher order scattering by larger QDs. This turns out to be necessary if the separation between bare exciton states belonging to different multiplets becomes comparable to the optical phonon energies. Experimental measurements of the absolute values of the scattering peak intensities would be very helpful for the correct determination of the exciton-phonon interaction constants from Raman spectra.

ACKNOWLEDGMENTS

This work was partially supported by the FCT (Portugal) through project POCI/FIS/58524/2004 and by the EC Project Ref. 505285-1 "SEMINANO." R.P.M. wishes to acknowledge the FMNC group of the Center of Physics of the University of Minho.

APPENDIX

In the strong confinement regime, the unperturbed exciton wave functions are well-described by products of the electron and hole ones,

$$\Psi_{\sigma,M}(\mathbf{r}_e,\mathbf{r}_h)=\Psi^e_\sigma(\mathbf{r}_e)\Psi^h_M(\mathbf{r}_h). \tag{A1}$$

For wide-gap semiconductors, such as CdSe, the confined electron and hole levels may be treated independently. For electrons near the bottom of the conduction band, it is sufficient to consider a single parabolic band in the framework of the effective mass approximation. It is possible to show that the wave functions corresponding to the electron ground state are given by[34]

$$\Psi^e_\sigma(\mathbf{r})=\left(\frac{2}{R}\right)^{1/2}\frac{\sin(\pi r/R)}{r}Y_{00}(\Omega)u^c_\sigma\equiv\psi_e(r)Y_{00}(\Omega)u^c_\sigma, \tag{A2}$$

where $Y_{lm}(\Omega)$ are the spherical harmonics and u^c_σ denotes the Bloch functions of the conduction band. For holes near the top of the valence band, the spherical approximation of the Luttinger-Kohn model[16] provides a good description of the confined states. Neglecting the spin-orbit split-off valence band, the wave functions which represent the hole ground state can be written as[20,35]

$$\Psi^h_M(\mathbf{r})=\Psi^{(0)}_M(\mathbf{r})+\Psi^{(2)}_M(\mathbf{r}), \tag{A3}$$

with

$$\Psi^{(0)}_M(\mathbf{r})=R_0(r)Y_{00}(\Omega)u^v_M, \tag{A4}$$

$$\Psi^{(2)}_{1/2}(\mathbf{r})=\frac{R_2(r)}{\sqrt{5}}\{Y_{20}(\Omega)u^v_{1/2}-\sqrt{2}[Y_{2,-1}(\Omega)u^v_{3/2}+Y_{22}(\Omega)u^v_{-3/2}]\}, \tag{A5}$$

$$\Psi^{(2)}_{-1/2}(\mathbf{r})=\frac{R_2(r)}{\sqrt{5}}\{Y_{20}(\Omega)u^v_{-1/2}-\sqrt{2}[Y_{21}(\Omega)u^v_{-3/2}+Y_{2,-2}(\Omega)u^v_{3/2}]\}, \tag{A6}$$

$$\Psi^{(2)}_{3/2}(\mathbf{r})=\frac{R_2(r)}{\sqrt{5}}\{-Y_{20}(\Omega)u^v_{3/2}+\sqrt{2}[Y_{21}(\Omega)u^v_{1/2}-Y_{22}(\Omega)u^v_{-1/2}]\}, \tag{A7}$$

$$\Psi^{(2)}_{-3/2}(\mathbf{r})=\frac{R_2(r)}{\sqrt{5}}\{-Y_{20}(\Omega)u^v_{-3/2}+\sqrt{2}[Y_{2,-1}(\Omega)u^v_{-1/2}-Y_{2,-2}(\Omega)u^v_{1/2}]\}, \tag{A8}$$

and u^v_M being the Bloch functions of the fourfold degenerate valence band Γ_8. The radial functions $R_l(r)$ are given by

$$R_0(r) = \frac{A}{R^{3/2}}\left[j_0(\kappa r/R) - \frac{j_0(\kappa)}{j_0(\beta^{1/2}\kappa)} j_0(\beta^{1/2}\kappa r/R) \right] \quad \text{(A9)}$$

and

$$R_2(r) = \frac{A}{R^{3/2}}\left[j_2(\kappa r/R) + \frac{j_0(\kappa)}{j_0(\beta^{1/2}\kappa)} j_2(\beta^{1/2}\kappa r/R) \right], \quad \text{(A10)}$$

where A is a normalization constant determined through the condition $\int_0^R [R_0^2(r)+R_2^2(r)]r^2dr=1$.

The electron-hole exchange interaction and the intrinsic crystal field lead to the perturbations[21,36]

$$H_{exc} = -\frac{2}{3}\varepsilon_{exc} a_0^3 \delta(\mathbf{r}_e - \mathbf{r}_h)\boldsymbol{\sigma}\cdot\mathbf{J} \quad \text{(A11)}$$

and

$$H_{cr} = -\frac{\Delta_{cr}}{2}\left(M^2 - \frac{1}{4}\right), \quad \text{(A12)}$$

respectively, where $\boldsymbol{\sigma}$ denotes the vector of electron Pauli spin-1/2 matrices and $\mathbf{J}$ is the vector of hole spin-3/2 matrices. Using the transformation matrix

$$\begin{pmatrix} 0 & 0 & 0 & 0 & 0 & 0 & 1 & 0 \\ 0 & 0 & a^- & a^+ & 0 & 0 & 0 & 0 \\ 1/\sqrt{2} & 1/\sqrt{2} & 0 & 0 & 0 & 0 & 0 & 0 \\ 0 & 0 & 0 & 0 & a^+ & a^- & 0 & 0 \\ 0 & 0 & -ia^+ & ia^- & 0 & 0 & 0 & 0 \\ -i/\sqrt{2} & i/\sqrt{2} & 0 & 0 & 0 & 0 & 0 & 0 \\ 0 & 0 & 0 & 0 & -ia^- & ia^+ & 0 & 0 \\ 0 & 0 & 0 & 0 & 0 & 0 & 0 & 1 \end{pmatrix}, \quad \text{(A13)}$$

where

$$a^{\pm} = \left(\frac{\sqrt{16\eta^2 + \Delta^2 - 4\eta\Delta} \pm (2\eta - \Delta)}{2\sqrt{16\eta^2 + \Delta^2 - 4\eta\Delta}} \right)^{1/2}, \quad \text{(A14)}$$

one diagonalizes the exciton Hamiltonian with H_{exc} and H_{cr} included and provides the energies (32).

For the sake of completeness, we reproduce here the necessary results for optical phonons confined in a nanosphere, previously obtained in the framework of the continuum lattice dynamics model in Refs. 25 and 27. The equation for the eigenfrequencies, ω, of the confined modes with angular momentum l_p is

$$\begin{aligned} qRj_{l_p}'(qR)\{\gamma\epsilon_\infty[-kRg_{l_p}'(kR) + l_p g_{l_p}(kR)] + \delta_{l_p}[kRg_{l_p}'(kR) \\ + g_{l_p}(kR)]\} - l_p(l_p+1)j_{l_p}(qR)\{\gamma\epsilon_h[kRg_{l_p}'(kR) \\ - l_p g_{l_p}(kR)] + \delta_{l_p} g_{l_p}(kR)\} = 0, \end{aligned} \quad \text{(A15)}$$

where $q=\sqrt{(\omega_L^2-\omega^2)/\beta_L}$, $k=\sqrt{|(\omega_T^2-\omega^2)/\beta_T|}$, $\gamma=(\omega_L^2-\omega_T^2)/(\omega^2-\omega_T^2)$, $\delta_{l_p}=[l_p\epsilon_\infty+(l_p+1)\epsilon_h]$, β_L, ω_L, β_T, and ω_T are the curvature parameters and Γ-point frequencies of the bulk LO and TO phonon dispersion curves, ϵ_h is the dielectric constant of the matrix, and $g_l(x)$ is either $j_l(x)$ or $i^{-l}j_l(ix)$ depending on the sign of $[(\omega_T^2-\omega^2)/\beta_T]$ (for "+" and "−," respectively). For $l_p=0$ Eq. (A15) reduces to

$$\tan(qR) = qR. \quad \text{(A16)}$$

The electrostatic potential associated with the confined mode $(n_p l_p m_p)$, inside the dot $(r<R)$ is given by

$$\varphi_{n_p l_p m_p}(\mathbf{r}) = \frac{C_F}{e}\Phi_{n_p l_p}(r) Y_{l_p m_p}(\Omega)$$

with

$$\Phi_{n_p 0}(r) = \sqrt{2}\frac{j_0(x_{n_p}) - j_0(x_{n_p} r/R)}{|\sin(x_{n_p})|} \quad \text{(A17)}$$

for $l_p=0$, and

$$\Phi_{n_p l_p}(r) = A_{n_p l_p}[j_{l_p}(qr) + S_1\gamma^{-1}(r/R)^{l_p}] \quad \text{(A18)}$$

for $l_p>0$, where the normalization constant is given by

$$\begin{aligned} A_{n_p l_p} = \Bigg\{ \int_0^1 \Bigg\{ \Bigg[x_{n_p} j_{l_p}'(x_{n_p} t) + S_1 l_p t^{l_p-1} + S_2 l_p(l_p+1)\frac{g_{l_p}(y_{n_p} t)}{t} \Bigg]^2 + l_p(l_p+1)\Bigg[\frac{j_{l_p}(x_{n_p} t)}{t} + S_1 t^{l_p-1} + S_2\Bigg(\frac{g_{l_p}(y_{n_p} t)}{t} \\ + y_{n_p} g_{l_p}'(y_{n_p} t)\Bigg)\Bigg]^2 \Bigg\} t^2 dt \Bigg\}^{-1/2}, \end{aligned}$$

$$S_1 = \frac{x_{n_p} j_{l_p}'(x_{n_p})[g_{l_p}(y_{n_p}) + y_{n_p} g_{l_p}'(y_{n_p} t)] - l_p(l_p+1) j_{l_p}(x_{n_p}) g_{l_p}(y_{n_p})}{l_p[l_p g_{l_p}(y_{n_p}) - y_{n_p} g_{l_p}'(y_{n_p} t)]}$$

and

$$S_2 = \frac{l_p j_{l_p}(x_{n_p}) - x_{n_p} j'_{l_p}(x_{n_p})}{l_p[l_p g_{l_p}(y_{n_p}) - y_{n_p} g'_{l_p}(y_{n_p} t)]}.$$

In the above expressions $x_{n_p}=qR$ and $y_{n_p}=kR$ correspond to the n_pth root of Eq. (A15) [or Eq. (A16) for $l_p=0$]. Note that outside the dot ($r>R$) the potential vanishes for $l_p=0$ and drops as r^{-l_p-1} for $l_p>0$.

Using the above expressions for the exciton wave functions and the phonon potential (A17) and (A18), the exciton-phonon interaction matrices can be easily calculated (they have been presented in Ref. 26 using a different notation). With the transformation (A13), it is not difficult to obtain the corresponding matrices in the $0^{U,L}$, $\pm 1^{U,L}$, and ± 2 representation (in this order). For $l_p=2$, these matrices are

$$B^{(n_p 2,0)} = J_{n_p 2} \begin{pmatrix} 1 & 0 & 0 & 0 & 0 & 0 & 0 & 0 \\ 0 & 1 & 0 & 0 & 0 & 0 & 0 & 0 \\ 0 & 0 & -b & c & 0 & 0 & 0 & 0 \\ 0 & 0 & c & b & 0 & 0 & 0 & 0 \\ 0 & 0 & 0 & 0 & -b & -c & 0 & 0 \\ 0 & 0 & 0 & 0 & -c & b & 0 & 0 \\ 0 & 0 & 0 & 0 & 0 & 0 & -1 & 0 \\ 0 & 0 & 0 & 0 & 0 & 0 & 0 & -1 \end{pmatrix}, \tag{A19}$$

$$B^{(n_p 2,1)} = -(B^{(n_p 2,-1)})^\dagger = J_{n_p 2} \begin{pmatrix} 0 & 0 & a^+ & -a^- & 0 & 0 & 0 & 0 \\ 0 & 0 & -a^+ & a^- & 0 & 0 & 0 & 0 \\ 0 & 0 & 0 & 0 & 0 & 0 & \sqrt{2}a^- & 0 \\ 0 & 0 & 0 & 0 & 0 & 0 & \sqrt{2}a^+ & 0 \\ -a^+ & -a^+ & 0 & 0 & 0 & 0 & 0 & 0 \\ -a^- & -a^- & 0 & 0 & 0 & 0 & 0 & 0 \\ 0 & 0 & 0 & 0 & 0 & 0 & 0 & 0 \\ 0 & 0 & 0 & 0 & -\sqrt{2}ia^- & \sqrt{2}ia^+ & 0 & 0 \end{pmatrix}, \tag{A20}$$

and

$$B^{(n_p 2,2)} = (B^{(n_p 2,-2)})^\dagger = J_{n_p 2} \begin{pmatrix} 0 & 0 & 0 & 0 & 0 & 0 & -1 & 0 \\ 0 & 0 & 0 & 0 & 0 & 0 & -1 & 0 \\ 0 & 0 & 0 & 0 & 0 & 0 & 0 & 0 \\ 0 & 0 & 0 & 0 & 0 & 0 & 0 & 0 \\ 0 & 0 & -\sqrt{2}c & -\sqrt{2}b & 0 & 0 & 0 & 0 \\ 0 & 0 & \sqrt{2}b & -\sqrt{2}c & 0 & 0 & 0 & 0 \\ 0 & 0 & 0 & 0 & 0 & 0 & 0 & 0 \\ -i & i & 0 & 0 & 0 & 0 & 0 & 0 \end{pmatrix}, \tag{A21}$$

where

$$b = \frac{2\eta - \Delta}{\sqrt{16\eta^2 + \Delta^2 - 4\eta\Delta}} \tag{A22}$$

and

$$c = \frac{2\sqrt{3}\eta}{\sqrt{16\eta^2 + \Delta^2 - 4\eta\Delta}}. \tag{A23}$$

The dimensionless coupling constants appearing in the expressions for the scattering probability are given by $\beta_{ll'}^{(\nu)} = B_{ll'}^{(\nu)}/(\hbar\omega_\nu)$.

*Electronic address: mikhail@fisica.uminho.pt

[1] *Nano-Optoelectronics. Concepts, Physics and Devices*, edited by M. Grundmann (Springer, Berlin, 2002).
[2] S. Hameau, Y. Guldner, O. Verzelen, R. Ferreira, G. Bastard, J. Zeman, A. Lemaître, and J. M. Gérard, Phys. Rev. Lett. **83**, 4152 (1999).
[3] E. Deleporte, S. Hameau, J. N. Isaia, Y. Guldner, O. Verzelen, R. Ferreira, G. Bastard, J. Zeman, and J. M. Gérard, Phys. Status Solidi C **1**, 1391 (2004).
[4] S. Sauvage, P. Boucaud, R. P. S. M. Lobo, F. Bras, G. Fishman, R. Prazeres, F. Glotin, J. M. Ortega, and J. M. Gérard, Phys. Rev. Lett. **88**, 177402 (2002).
[5] M. I. Vasilevskiy, E. V. Anda, and S. S. Makler, Phys. Rev. B **70**, 35318 (2004).
[6] E. Menéndez-Proupin, J. L. Pena, and C. Trallero-Giner, Semicond. Sci. Technol. **13**, 871 (1998).
[7] M. Cardona, in *Light Scattering in Solids II*, edited by M. Cardona and G. Güntherodt, Topics in Applied Physics, Vol. 50 (Springer-Verlag, Heidelberg, 1982); A. Cantarero, C. Trallero-Giner, and M. Cardona, Phys. Rev. B **39**, 8388 (1989); C. Trallero-Giner, A. Cantarero, and M. Cardona, Phys. Rev. B **40**, 4030 (1989).
[8] M. C. Klein, F. Hache, D. Ricard, and C. Flytzanis, Phys. Rev. B **42**, 11123 (1990).
[9] T. D. Krauss and F. W. Wise, Phys. Rev. B **55**, 9860 (1997).
[10] C. Trallero-Giner, A. Debernardi, M. Cardona, E. Menéndez-Proupin, and A. I. Ekimov, Phys. Rev. B **57**, 4664 (1998).
[11] Y.-N. Hwang, S.-H. Park, and D. Kim, Phys. Rev. B **59**, 7285 (1999).
[12] M. Yu. Ladanov, A. G. Milekhin, A. I. Toropov, A. K. Bakarov, A. K. Gutakovskii, D. A. Tenne, S. Schulze, and D. R. T. Zahn, J. Exp. Theor. Phys. **101**, 554 (2005).
[13] R. Rodríguez-Suárez, E. Menéndez-Proupin, C. Trallero-Giner, and M. Cardona, Phys. Rev. B **62**, 11006 (2000).
[14] E. P. Pokatilov, S. N. Klimin, V. M. Fomin, J. T. Devreese, and F. W. Wise, Phys. Rev. B **65**, 75316 (2002).
[15] M. I. Vasilevskiy, R. P. Miranda, E. V. Anda, and S. S. Makler, Semicond. Sci. Technol. **19**, S312 (2004).
[16] J. M. Luttinger and W. Kohn, Phys. Rev. **97**, 869 (1955).
[17] W. Hayes and R. Loudon, *Scattering of Light by Crystals* (Wiley, New York, 1978).
[18] R. J. Elliott, Phys. Rev. **108**, 1384 (1957).
[19] G. D. Mahan, *Many-Particle Physics* (Kluwer Academic, New York, 2000).
[20] A. I. Ekimov, F. Hache, M. C. Schanne-Klein, D. Ricard, C. Flytzanis, I. A. Kudryavtsev, T. V. Yazeva, A. V. Rodina, and Al. L. Efros, J. Opt. Soc. Am. B **10**, 100 (1993).
[21] D. J. Norris and M. G. Bawendi, Phys. Rev. B **53**, 16338 (1996).
[22] Al. L. Efros, M. Rosen, M. Kuno, M. Nirmal, D. J. Norris, and M. Bawendi, Phys. Rev. B **54**, 4843 (1996).
[23] V. V. Sobolev, V. I. Donetskina, and E. F. Zagainov, Sov. Phys. Semicond. **12**, 646 (1978).
[24] N. Miura, G. Kido, and S. Chikazumi, in *Proceedings of the 14th International Conference on the Physics of Semiconductors, Edinburgh, 1978*, edited by B. L. H. Wilson (IOP Publishing, Bristol, 1979), p. 1109.
[25] M. P. Chamberlain, C. Trallero-Giner, and M. Cardona, Phys. Rev. B **51**, 1680 (1995).
[26] V. M. Fomin, V. N. Gladilin, J. T. Devreese, E. P. Pokatilov, S. N. Balaban, and S. N. Klimin, Phys. Rev. B **57**, 2415 (1998).
[27] M. I. Vasilevskiy, Phys. Rev. B **66**, 195326 (2002).
[28] M. Babiker, J. Phys. C **19**, 683 (1986).
[29] M. I. Vasilevskiy, E. V. Anda, and S. S. Makler, in *Proceedings of the 26th International Conference on the Physics of Semiconductors, Edinburgh, 2002*, edited by A. R. Long and J. H. Davies (IOP Publishing, Bristol, 2003), p. 229.
[30] M. I. Vasilevskiy, A. G. Rolo, M. J. M. Gomes, O. V. Vikhrova, and C. Ricolleau, J. Phys.: Condens. Matter **13**, 3491 (2001).
[31] C. Trallero-Giner, A. Alexandrou, and M. Cardona, Phys. Rev. B **38**, 10744 (1988).
[32] S. Schmitt-Rink, D. A. B. Miller, and D. S. Chemla, Phys. Rev. B **35**, 8113 (1987).
[33] V. I. Belitsky, A. Cantarero, S. T. Pavlov, M. Cardona, I. G. Lang, and A. V. Prokhorov, Phys. Rev. B **52**, 11920 (1995).
[34] L. E. Brus, J. Chem. Phys. **79**, 5566 (1983).
[35] J. B. Xia, Phys. Rev. B **40**, 8500 (1989).
[36] Al. L. Efros, Phys. Rev. B **46**, 7448 (1992).